Dynamic constitutional gold nanoparticles frameworks for carbonic anhydrase activation

Sanaa Daakour, Gihane Nasr, Mihail Barboiu

Dynamic constitutional gold nanoparticles frameworks for carbonic anhydrase activation

Sanaa Daakour,[1,2] Gihane Nasr,[2] Mihail Barboiu[1,3*]

[1]Institut Européen des Membranes, Adaptive Supramolecular, Nanosystems Group, University of Montpellier, ENSCM, CNRS, Place Eugène Bataillon, CC 047, F-34095, Montpellier, France. [2]Bioactive Molecules Research Laboratory, Department of Chemistry and Biochemistry, Faculty of Sciences, Section II, Lebanese University, Jdaidet el-Metn, B.P. 90656, Lebanon. [3] Babes-Bolyai University, Supramolecular Organic and Organometallic Chemistry Center (SOOMCC), Cluj-Napoca, 11 Arany Janos str., 400028, Cluj-Napoca, Romania.

KEYWORDS carbonic anhydrase, dynamic constitutional frameworks, enzyme activation, gold nanoparticles, self-assembly

Abstract: Dynamic constitutional materials are constructed from reversibly connecting components adaptively self-assembling under the pressure of internal or external factors. Functional macro-monomeric poly(ethyleneglycol) segments and 3D connecting cores can be used to conceive biomimetic dynamic constitutional frameworks (DCFs) for selective/adaptive biomolecular encapsulation of proteins, enzymes, etc. Gold nanoparticles (AuNps) can be involved as core connectors to expand the networks of DCFs at the nano-scale, thereby increase the biomolecular encapsulation and activity. Efficient encapsulation of bovine carbonic anhydrase (bCA) in host matrixes is of tremendous importance for maintaining its stability, catalytic activity and the durability. In this paper we demonstrate that AuNps-DCFs-bCA bioconjugates, synthesized via reversible imine/amino-carbonyl as sulfide-AuNps chemistries, assemble into nanometric aggregates of around 200 nm with high stability for bCA encapsulation. This system showed an impressive improved catalytic activity, more than 30 times higher than bCA alone. The K_m values were two to three times lower compared to free bCA indicating a stronger affinity for bCA under encapsulation, while V_{max} was higher. This performance is very promising for current state-of-the-art carbon dioxide capture systems with equivalent amounts of enzyme, even after heating for a prolonged period at 100°C, translating into a direct perspective for enhancing flue gas capture and conversion performances.

INTRODUCTION

Spontaneous reversible fabrication of Dynamic Constitutional Materials incorporating biomolecular components is an efficient and robust method to self-assemble individual components into functional objects with higher complexity and multiple responsiveness [1–3]. The programed self-assembled can be achieved by using polymers and nanoparticles with appropriate size and length that generate adaptive connections between components within materials with increased performances in a wide range of applications [4]. Polymers can control the connections within such structures offering functionality. The reversibility of interactions is an essential factor and can be particularly achieved at supramolecular and covalent levels by using Constitutional Dynamic Chemistry (CDC) principles[5]. The Dynamic Constitutional Frameworks (DCFs) involving reversible covalent connections between components may enable multivalent interactions within the materials [6] and synergistically modulate its overall self-organization when interacting with biological targets [7,8]. Meanwhile, nanoparticles can introduce magnetic, conductive, light modulating behaviors or thermal stability to the assemblies [9].

Among the nanoparticles, gold nanoparticles (AuNps) have attracted substantial interest due to their easy synthesis and functionalization, chemical stability, biocompatibility and tunable optoelectronic properties (absorption, fluorescence, conductivity)[10]. Although there are many examples of self-assembled AuNps using covalent bonds [11] and reversible supramolecular interactions [12,13], as far as we know, there are no examples of AuNps connected *via* Dynamic Constitutional Frameworks (DCFs) that can interact with biomolecules and that could bring new functions for the nanostructured assemblies [5,14,15].

Natural enzymes present inherent drawbacks such as easy inactivation, moderate stability outside cell environment, thus their immobilization within protecting matrixes can adjust their activity and stability [16,17]. A solution to achieve effective catalytic performance for enzymes is the development of nanohybrid biocatalysts which involve the combination of nanoparticles and biomolecules (DNA, enzymes) [18]. The incorporation of platinum nanoparticles with aminopeptidase [19] or uricase[20] has been found to preserve a high level of catalytic activity. This highlights the immense potential of artificial metalloenzymes across a range of applications. Carbonic anhydrases (CAs), in particular, are widely spread metalloenzymes in all life kingdoms, being implicated in crucial physiologic processes, as they catalyze a simple but fundamental reaction, the reversible hydration of carbon dioxide to bicarbonate and protons [21]. A wide range of materials were explored for CA immobilization including chitosan, hydrogels, metallic nanoparticles, etc. [22]. Colloidal bovine bCA- or human hCA-AuNps [23] assembled to amine/thiol functionalized SBA-15 support maintain the enzymatic activity [24].

In our previous work, a straightforward approach for CA encapsulation based on the direct addition into an aqueous solution containing the CA enzyme of interactive poly(ethyleneglycol) PEGylated DCFs linked with reversible imine bonds and equipped with H-bonding motifs, showing not only enzyme protection effect, but also important activation effects towards CA activity in aqueous solution [25]. Our strategy excludes enzyme chemical modifications, formation of covalent attachment points, or adsorption on non-specific sites, as compared to classic immobilization techniques. The *in situ* reversible generation of DCFs adaptively encapsulate CA through H-bonding and imine-bond formation on the enzyme surface. It is generating a "protective encapsulating" layer around the enzyme, leading to stabilized tertiary protein structures in solution and providing proximal multivalent proton acceptor groups in the close proximity of the enzyme surface, assisting the proton shuttling during the catalytic cycle.

Herein, we anticipated that gold nanoparticles (AuNps) can be used as constitutive "bricks", to extend the assembly of Carbonic Anhydrase / Dynamic combinatorial frameworks (DCFs) located at the nanoscale. This combination offers an interesting platform toward materials for environmental applications exploiting the advantage of the dynamic enzyme encapsulation at the nanoscale offered by reticular space between self-assembled AuNps filled with functional compartmentalized DCFs, embedding activated Carbonic Anhydrase enzyme (**Figure 1**).

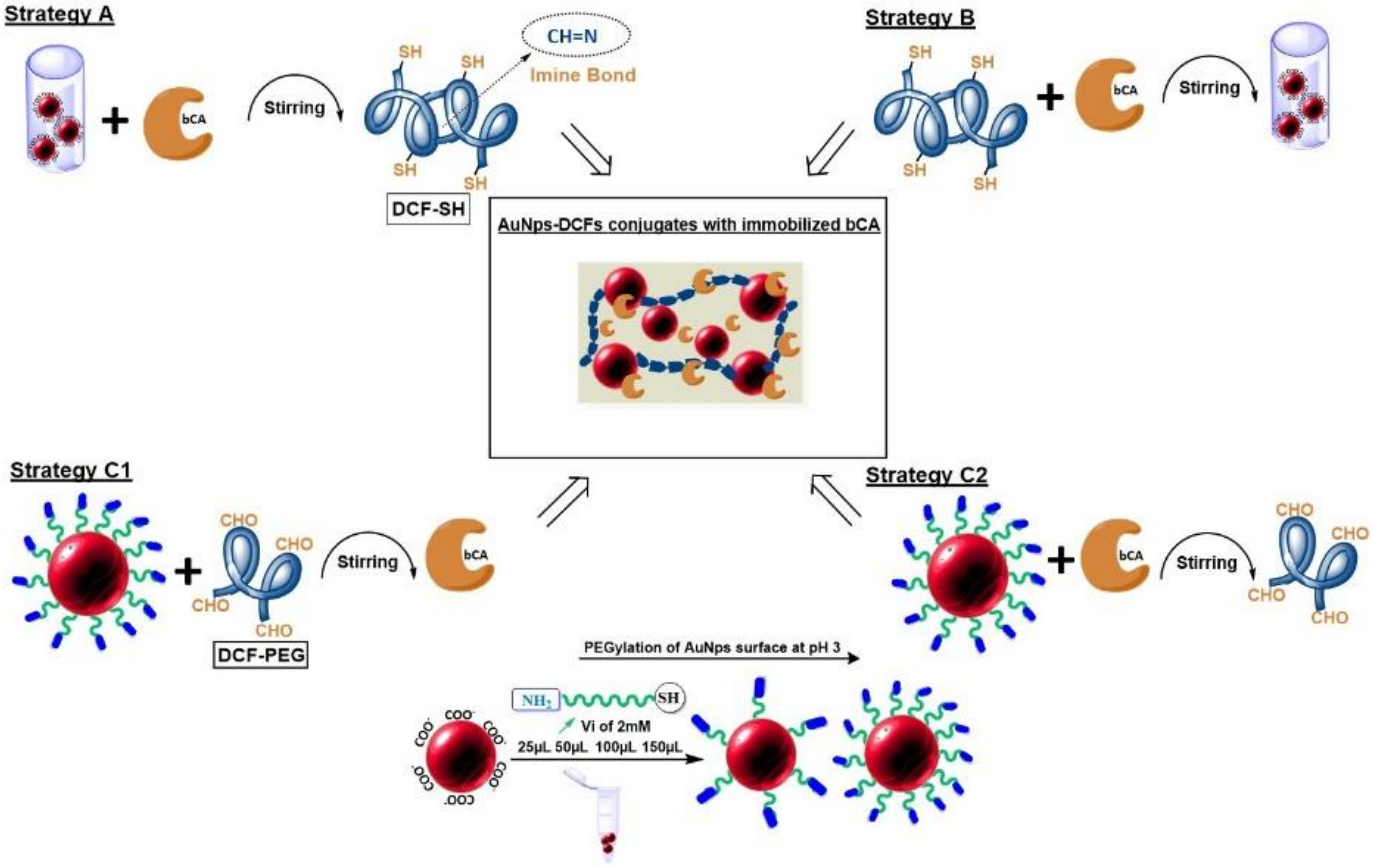

Figure 1. Schematic representation of the design fabrication strategies used to encapsulate bCA in AuNps-DCFs conjugates.

RESULTS

Design, synthesis and characterization of Citrate-, HS-PEG$_{2000}$- NH$_2$, DCF-SH- and DCF-PEG- stabilized AuNps: Gold nanoparticles were synthesized thoroughly the reduction of $HAuCl_4$ by citrate where the latest plays a double role as reducer and stabilizer (**Figure S1**) [26]. The DCF-SH frameworks were obtained *via* reversible amino/carbonyl-imine chemistry by reacting benzene-1,3,5-tricarbaldehyde and amino-terminated-poly(ethyleneglycol) NH$_2$-PEG$_{1500}$-NH$_2$ and thiol-poly(ethylene-glycol)amino-terminated HS-PEG$_{2000}$-NH$_2$ macromonomers (**Figure S2**). These macromonomers are highly water soluble and serve as biocompatible chaperones for refolding and limiting aggregation of bovine carbonic anhydrase (bCA) [27]. DCF-SH was then used to enable the exchange with citrate on the surface of AuNps [28]. The NMR spectra confirm the formation of dynameric mixtures, as observed from analysis of multiple peaks ~8 ppm, representing the aromatic and imines protons (**Figure S7, S8**). These can confirm the cross-linking between core centers and amine compounds through imine formation reaction. DOSY spectra previously indicated the approximate average molecular weights of dynamers were 40000 g/mol[25] The interactions of DCF-SH on AuNps surface and their reconstruction in presence of particles through the "grafting to" approach created stable and soluble AuNps-DCFs conjugates. In parallel, we developed a "grafting from"

approach based on the PEGylation of AuNps that results in the formation of NH_2-PEG_{2000}-SHAuNps, presenting amino groups on the surface that can react with free aldehyde DCFs constructed from benzene-1,3,5-tricarbaldehyde and H_2N-PEG_{1500}-NH_2. Finally, bCA was encapsulated within the AuNps-DCFs conjugates **(Figure 1)**: bCA was added with AuNps then mixed with DCF-SH (strategy A), or added with DCF-SH then mixed with AuNps (strategy B), mixed directly with DCFs network and then with NH_2-PEG_{2000}-SH-AuNps (strategy C1), or mixed first with NH_2-PEG_{2000}-SHAuNps and then with DCF-PEG (strategy C2). The AuNps-DCFs conjugates were qualitatively analyzed in aqueous solution and solid state: size, morphology, and surface plasmon resonance band. The catalytic activity of DCFs, AuNps-DCFs conjugates and free or encapsulated bCA were evaluated by using the model hydrolysis reaction of *p*-nitrophenyl acetate (*p*-NPA), following the formation of the *p*-nitrophenol (*p*-NP) product by UV-vis spectroscopy (**Figure S12**) [25].

The "grafting to" self-assembly approach of citrate-stabilized gold nanoparticles of 22.1 ± 0.2 nm diameter with thiol decorated DCF-SH is highly dependent of the used amount of DCFs. The charge surface of AuNps, the pH, and ligand is modulating the interaction with aqueous DCFs solution.

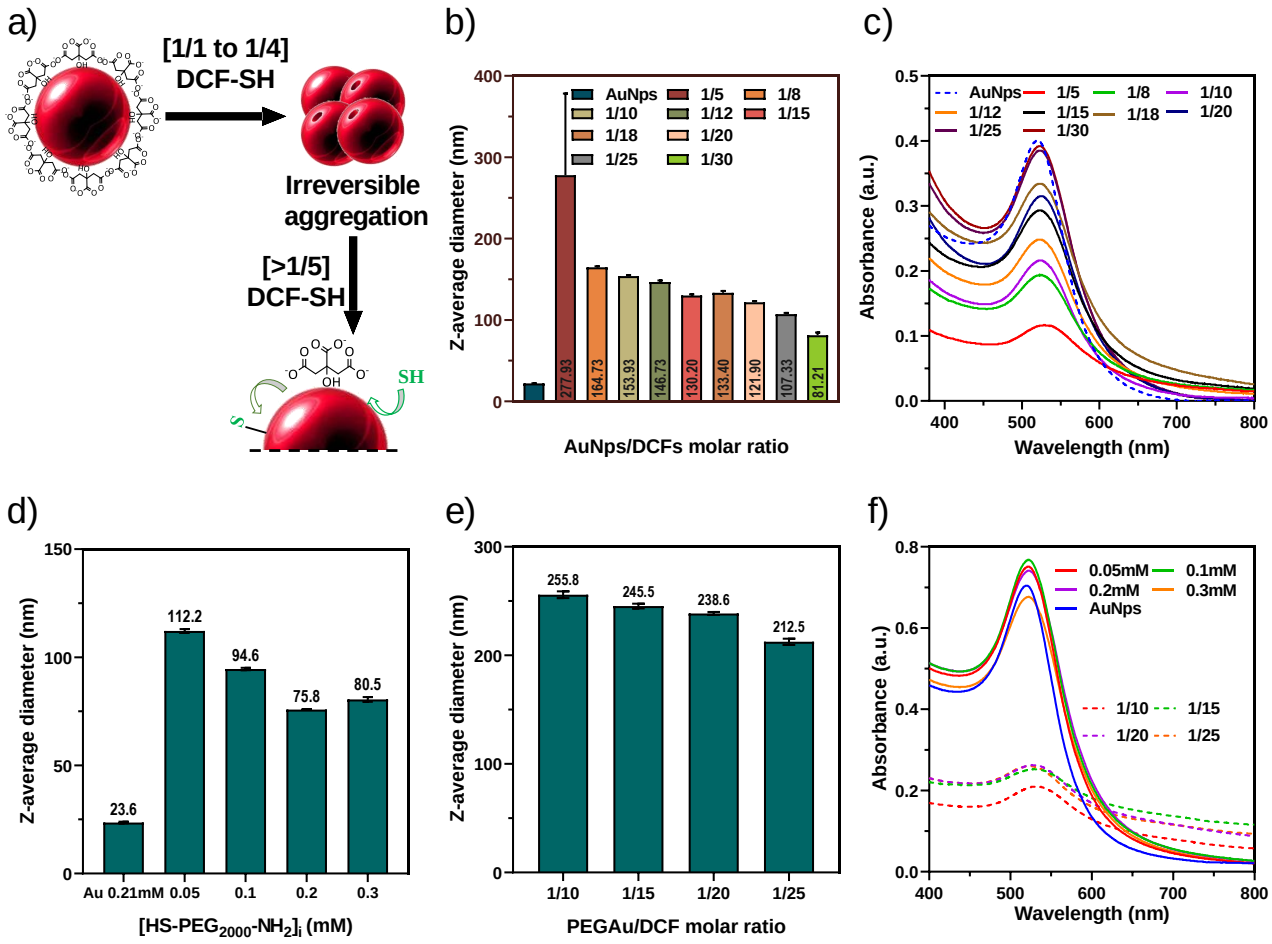

Figure 2. a) Schematic representation of the citrate exchange reactions with DCF-SH on the surface of AuNps leading to stable assemblies starting from 1/5 AuNps/DCFs molar ratio. b) Z-average diameter, measured by DLS, at different AuNps to DCFs molar ratios. c) Surface plasmon resonance band detected around 520 nm for 0.21 mM AuNps in presence of DCF-SH (n=3; mean ± SD). d) Z-average diameter measured by DLS of PEG-AuNps in presence of increasing amount of HS-PEG_{2000}-NH_2. e) NH_2-PEG_{2000}-SHAuNps in presence of increasing amounts of DCF-PEG. f) Surface plasmon resonance band characteristic of gold nanoparticles for the samples d, e.

Free thiol groups of DCF-SH successfully displace the citrate and stabilized the particles in the suspension, due to the affinity of thiol molecules to gold surfaces **(Figure 2a)** [15]. Less gold cores-meaning smaller size- were implicated in the assembly of conjugates when the amount of DCFs increased because of more attachment of SH groups. Moreover, an increased hydrodynamic diameter confirmed the attachment of the DCF-SH on the surface of AuNps [28].

At low AuNps/DCF-SH molar ratios large sized conjugates of 277.9 nm diameter and a high polydispersity index PdI > 0.5 were formed most probably due to weak crosslinking on the Au surface [29]. The addition of increasing amounts of

DCF-SH leads to a decrease of the size of conjugates and of their polydispersity in water (PdI<0.5). For instance, at 1/10 AuNps/DCF-SH molar ratio the z-average diameter was 153.9 ± 1.24 nm and significantly decreased to 81 ± 3.44 nm at the highest ratio of 1/30 **(Figure 2b)**. The SH groups are important to assemble gold cores as shown by the slight increase of the size with free SH, DCF-PEG (BTA : PEG at 1:1.5 molar ratio) **(Figure S4,S5)**, mainly due to limited interactions on the surface of particles. A sharp and well-defined SPR band was detected for AuNps at 520 nm **(Figure 2c)**, which is characteristic of AuNps of 10 to 100 nm diameter [30]. This band was as well detected for all AuNps-DCFs conjugates around 520 nm, with a slight difference of shape and intensity. The peak width was increased in presence of small amount of DCF-SH, then decreased and simultaneously become similar to citrate-stabilized AuNps for higher amounts of DCF-SH, indicating a decrease of polydispersity in presence of adequate amounts of the polymer. While comparing the SPR peak of all AuNps-DCFs conjugates to citrate-AuNps, a small redshift (< 6 nm) was observed due to the formation of dielectric layers of alkanethiol on the surface [31]. However, while comparing this peak between conjugates of increased DCFs amounts, blueshifts were noticed thus the particle size decreased proportionally with the amount of DCFs [32].

Next the functionalization of AuNps with HS-PEG_{2000}-NH_2 was performed by exchanging the citrate on the gold surface in solution at pH=3 (**Figure S3**). The size of AuNps (23.6 nm) is significantly increasing to 112.2 nm (0.05 mM), then it is decreasing to 94.6 nm (0.1 mM) and 80 nm (0.2 - 0.3 mM) in presence of HS-PEG_{2000}-NH_2 **(Figure 2d)**. This observation confirms that PEGylation reaction is stabilized beyond a critical concentration. In presence of low amount of HS-PEG_{2000}-NH_2, the PEG tends to interact with nearby particles via strong SH Au^1-SH covalent bond and form high aggregates [33]. Higher amounts of HS-PEG_{2000}-NH_2, increased the Au-SH bonds while limiting the Au/PEG weak adsorption resulting in the formation of smaller soluble particles. The same behaviors were also observed in a study on methoxy-PEG-thiols of different molecular weights as the particles were stabilized by a capping layer of PEG beyond a crucial stability concentration (CSC) [34]. A characteristic redshift of approximately 2 nm of the initial SPR band of AuNps at 520 nm, was detected after HS-PEG_{2000}-NH_2 addition proving a successful functionalization while maintaining the particles in the suspension **(Figure 2f)**. The usage of PEG with a 2000M spacer in this particular step ensured a balance between achieving a high capping density and providing stability to the AuNps.

Then, the "grafting from" approach, was used to connect DCF-PEG with NH_2-PEG_{2000}-SHAuNps. DLS analysis demonstrated a significant increase by two and three times of the diameter of resulted AuNps-DCFs from 112.2 nm to 255.8 nm (molar ratio1/10), and from 80.5 nm to 212.5 nm (molar ratio 1/25) **(Figure 2e**, **Figure S6**). The SPR band of AuNps-DCFs conjugates was subjected to redshifts compared to citrate-AuNps and NH_2-PEG_{2000}-SHAuNps **(Figure 4f)**. The maximum wavelength was shifted to 530 nm for small ratios 1/10 and 1/15, then it was restored to 520 nm at 1/20 and 1/25 ratios. Besides, the shape of the band was significantly changed as we observed an enlarged width with a lower intensity. FTIR spectra confirm the successful formation of DCf and their connection to Au Nps -see supporting information (**Figure S9**). This demonstrates the interactions of DCFs with the surface of AuNps, modifying the local dielectric environment and electric charge induced the formation of extended conjugates.

Transmission Electronic Microscopy -TEM analysis of AuNps and AuNps-DCFs conjugates: TEM was used to observe the size along with shape and the aggregation behaviors of synthesized AuNps before and after addition of HS-PEG_{2000}-NH_2 or DCFs [35]. Citrate-AuNps show spherical morphology and good dispersion with a mean diameter of 12 nm as calculated from TEM **(Figure 3a, c)**. A decrease of sizes of dried samples prepared from diluted solutions on carbon grids for TEM experiments was noticed compared to DLS measurement showing the hydrodynamic diameter. Further functionalization of AuNps showed that surface modification HS-PEG_{2000}-NH_2 ligand lead to a homogeneous self-assembly of spherical particles of a mean diameter 13.4 nm **(Figure 3b,d)**. As seen in these micrographs, functionalized particles were linked together and the number of particles (frequency) in a specific area increased with higher amounts of HS-PEG_{2000}-NH_2. The PEG layer provided a steric stability on the surface that result in the formation of uniform films. TEM micrograph of AuNps assembled in presence of 0.21mM DCF-SH following the strategies A, B showed the formation of high aggregates where spherical particles are fused and inter-connected **(Figure 3e)**. **Figure 3f** shows TEM images of NH2-PEG_{2000}-SHAuNps combined to DCF-PEG, following the strategy C, where spherical particles were dispersed into aggregates, which individual particles fused together. Similar formation of regular aggregates was previously observed with the successful dispersion of AuNps in polystyrene (PS) and poly(dimethylsiloxane) (PDMS) polymeric matrices [36].

Binding DCFs and AuNps-DCFs conjugates to bCA: The intrinsic fluorescence of bCA, mostly due to its tryptophan residues, is highly sensitive to modifications of the surrounding environment, which make the fluorescence emission spectra suitable for its binding or conformational changes studies [37]. So we have used, fluorescence spectroscopy to provide relevant information and the binding or association constant (K_a) of bCA to citrate-AuNps, DCFs and AuNps-DCFs conjugates. Here, the fluorescence spectra of the bCA aqueous solutions, recorded between 250 and 500 nm, upon excitation at 280 nm, covering the emission band of tryptophan at 350 nm [38] and exhibiting a strong intrinsic fluorescence band centered at 347 nm. A strong fluorescence quenching effect and a small blueshift (7 nm), related to the polarity changes around tryptophan, were observed in presence of increasing concentration of AuNps **(Figure S10)**. The binding constant between AuNps and bCA determined by using the Stern-Volmer relation, is 14680 M^{-1} validating strong interactions of bCA on AuNps surface. Bovine serum albumin, is showing a same binding behavior in presence of citrate-AuNps, emphasizing the

importance of the electric charge of the metal surface and the inert nature of sodium citrate [39]. Interestingly, the shape of emission spectra of bCA was maintained, confirming that bCA remains in its native configuration with negligible conformational changes upon the addition of AuNps [40]. A similar quenching effect was noticed in presence of proportional DCF-SH concentrations **(Figure S10)**. Most probably DCF-SH binds *via* transamination with amino groups, disulfide S-S bond formation and poly(ethylene glycol)/bCA non-covalent interactions at the bCA surface [25,41] showing an association constant K_a of 2578M^{-1}.

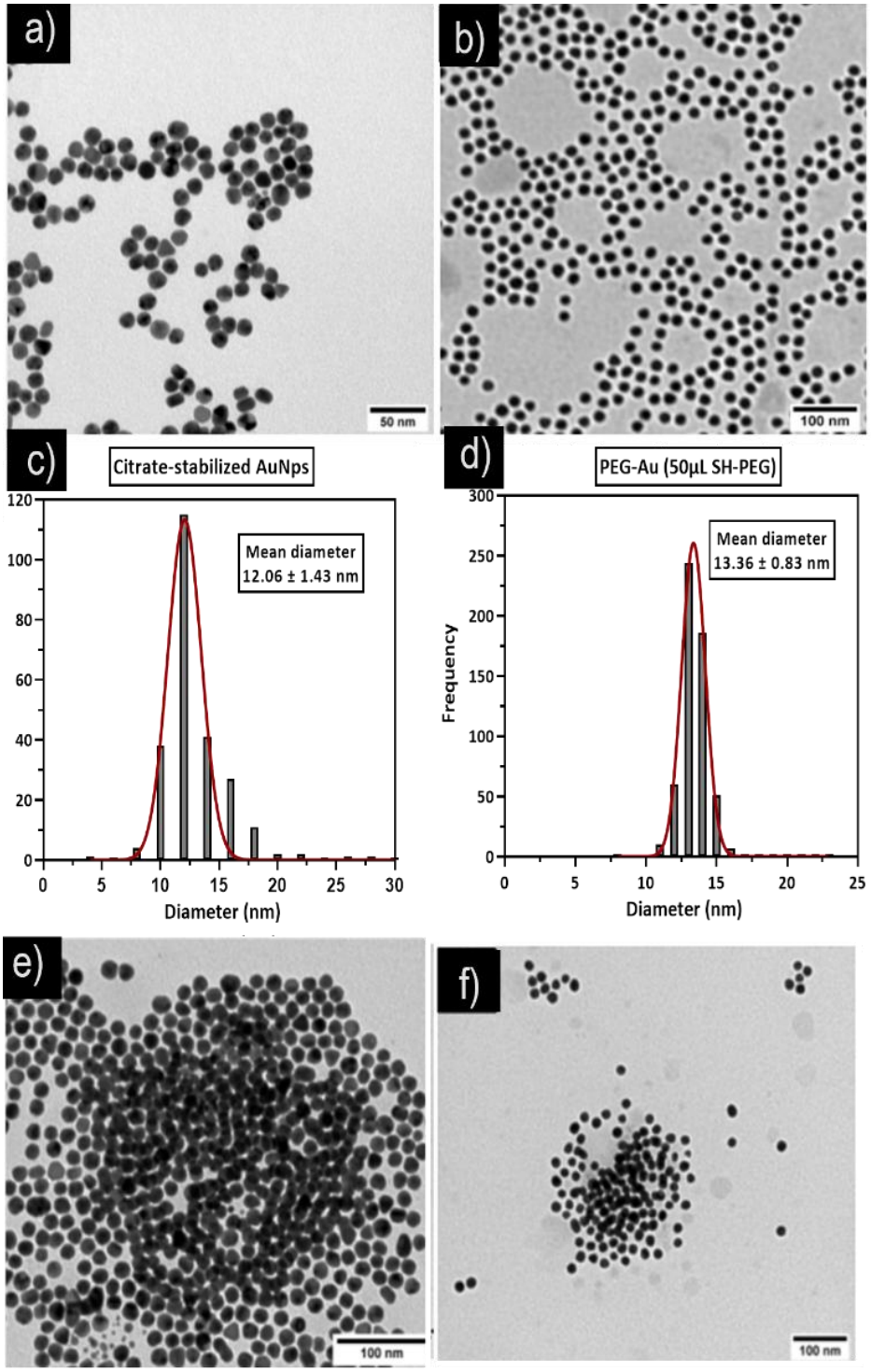

Figure 3. Representative TEM images and nanoparticle size distribution illustrating a, c) citrate-stabilized AuNps, b, d) NH_2-PEG_{2000}-SHAuNps, e) AuNps-DCFSH conjugates –strategies A,B and f) NH_2-PEG_{2000}-SHAuNps combined to DCF-PEG conjugates - strategy C.

The fluorescence experiments were conducted combining also variable concentrations of DCFs and constant concentrations of AuNps and bCA. We observed that the fluorescence spectra strongly differ following used strategy, relating to the initial contact of the components with bCA. Starting with the strategy A, initially getting bCA in contact with AuNps, we noticed a drastic change of the emission band showing an enlarged width and redshifts of the wavelength with increasing concentrations of DCF-SH, so we were unable to determine the biding constant **(Figure S11)**. Differently, by using the strategy B when bCA is initially contacted with DCFs – we observed a firm quenching effect, similar to the binding of DCFs or AuNps respectively **(Figure S10)**. We determined a binding constant K_a equal to 1170 M^{-1} while the bCA structure is maintained intact within the hybrid assembly. The lower binding K_a compared to free DCFs to bCA is explained by a synergetic interactions of DCFs with AuNps. The mechanism of binding could be described as follow: DCFs encapsulated bCA most probably *via* imine bond with CA surface amines and PEG interactions on the surface, then AuNps are able to interact with remaining SH groups of DCFs as well as some binding sites for bCA which are strongly reduced. On the other hand, in strategy A the addition of DCFs created a competitive environment for bCA strongly interacting on the surface of AuNps. Furthermore, bCA was efficiently bounded to the pre-formed PEGAuNps-DCFs conjugates (strategy C1) and displayed a higher K_a than the previous strategies of 1619 M^{-1}. The high density of PEG on the surface of AuNps and the larger size of these conjugates explains this significant binding affinity.**Catalytic activity of bCA, DCFs and AuNps-DCFs conjugates:** After demonstrating the ability of bCA to bind to AuNps, DCFs and AuNps-DCF conjugates, our next interest was to determine the catalytic activity all along the formulations used without and with immobilized bCA. The esterase activity through the hydrolysis reaction of *p*-NPA is directly related to CO_2 hydration reaction catalyzed by both bCA and AuNps-DCFs systems. The absorbance at λ=400 nm was monitored to estimate the catalytic activity relative to the reference activity of free bCA in solution at different concentrations of components (**Figure S13**).

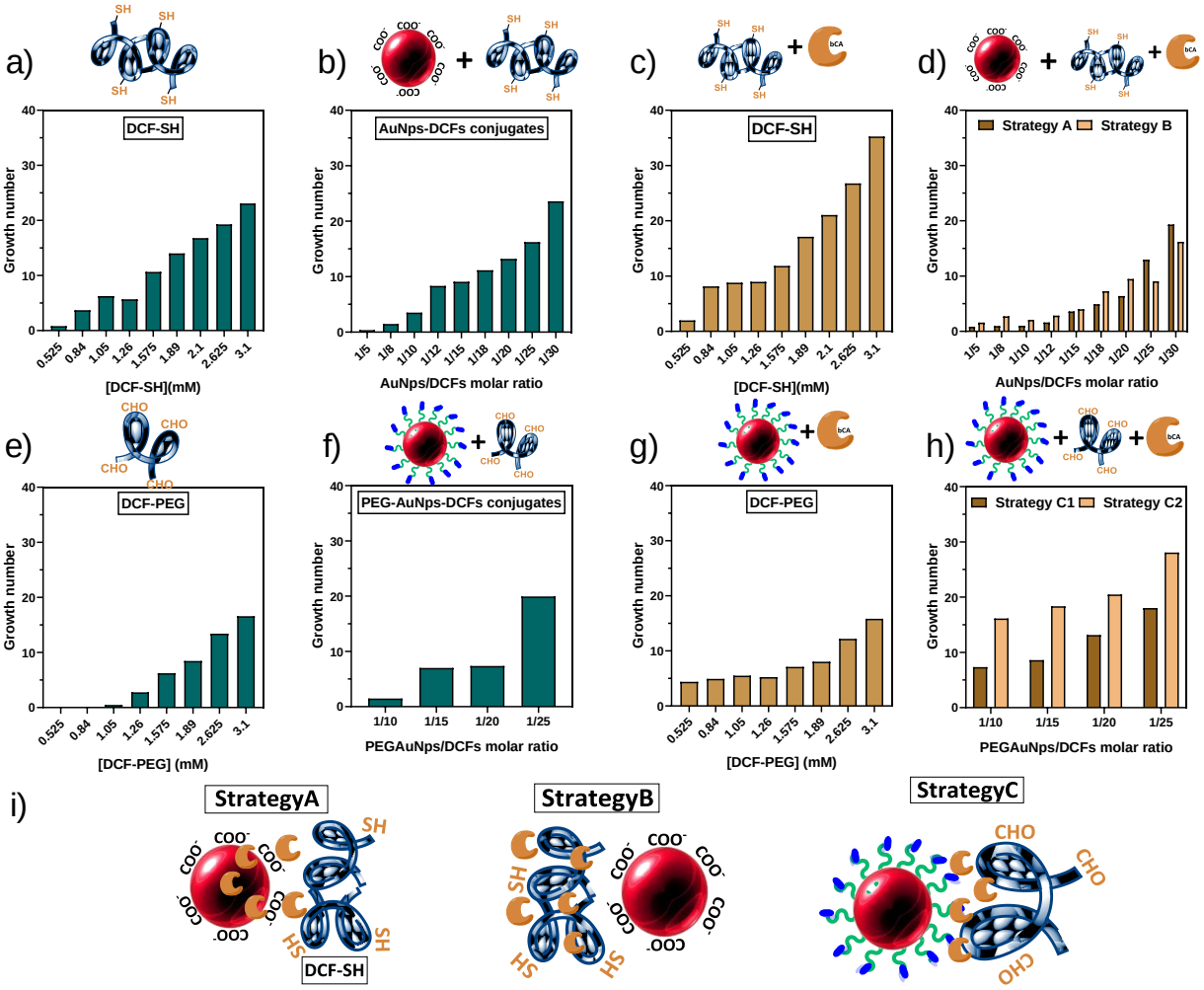

Figure 4. Hydrolysis of *p*-NPA, monitored by Growth number calculated the rate of increase of the activity relative to the free bCA with the addition of a) DCF-SH, b) AuNps-DCF-SH, c) DCF-SH-bCA d) AuNps-DCFSH-bCA, e) DCF-PEG, f) NH_2-

PEG_{2000}-SHAuNps-DCF-PEG, g) DCF-PEG-bCA and h) NH_2-PEG_{2000}-SHAuNps-DCF-PEG-Bca, i) Possible interactional mechanisms of bCA within AuNps-DCFs conjugates assembled through strategies A, B, and C.

Interestingly, the DCF-PEG and DCF-SH frameworks present an increasing activity proportionally to the amount of added DCFs **(Figure S14, S15).** We defined a growth number that calculate the rate of increase of the catalytic activity relative to the rate of free bCA. This activation is more pronounced in presence of DCF-SH **(Figure 4a)** than DCF-PEG **(Figure 4e)**. This emphasize the importance of stronger nucleophilic SH groups present in HS-PEG_{2000}-NH_2 when compared with amino groups of H_2N-PEG_{2000}-NH_2 that strongly contributing as to an enhanced catalytic activity on the hydrolysis of *p*-NPA. The increase of catalytic activities are maintained when DCF-SH (**Figure 4b**) and DCF-PEG (**Figure 4f**) are interacting with AuNps, reminiscent with optimal availability of the catalytic -SH and NH_2 groups despite the presence of AuNps. The addition of constant amount of bCA to increasing ratios of DCF-SH and DCF-PEG induce substantial up to 50% increase in the catalytic activity of DCFs-bCA bioconjugates at high DCFs ratios (**Figure 4c,g**). Interestingly, at low concentration between 0.525 and 1.575 mM DCFs, we note that observed increased activity is coming from bCA alone as DCFs themselves do not present any activity. Most probably, this is the results of complex cooperative effects relied to the formation of imine or disulfide bonds assisted by PEG non-covalent self-assembly on the surface of the bCA, that are able to reduce the mobility of the enzyme under such confined conditions in the solution and concomitantly play the role of shuttling out the protons from the zinc-active site, as previously observed [25,41]. The DCFs could be advantageous for the immobilization support where bCA activity is maintained and supplemented by the intrinsic catalysis effect of the support.

Next, the catalytic activity of bCA was monitored in AuNps-DCFs-bCA bioconjugates prepared *via* strategies A-C. For the strategies A and B (**Figure 4d**) where bCA is in contact initially with AuNps or with DCF-SH (**Figure 4c**), respectively, the catalytic activity is decreasing when compared with the activity observed with DCF-SH-bCA bioconjugates in the absence of AuNps. Most probably the formation of low compact aggregates between AuNps and DCF-SH observed in solution by DLS (**Figure 2b**) are responsible for the lower growth numbers observed for such systems where the bCA is most probably less immobilized in the bioconjugates. At low ratios of AuNps/DCFs the growth numbers are lower upon strategy A where bCA is in contact initially with AuNps than that observed with strategy B where bCA is in contact initially with DCF-SH. Then, NH_2-PEG_{2000}-SHAuNps were used to immobilize bCA in presence of DCF-PEG (strategy C). Here, two ways were adopted: bCA was added directly with the pre-made NH_2-PEG_{2000}-SHAuNps-DCFs conjugates (strategy C1) or bCA was added with NH_2-PEG_{2000}-SHAuNps nanoparticles then mixed with DCF-PEG (strategy C2).

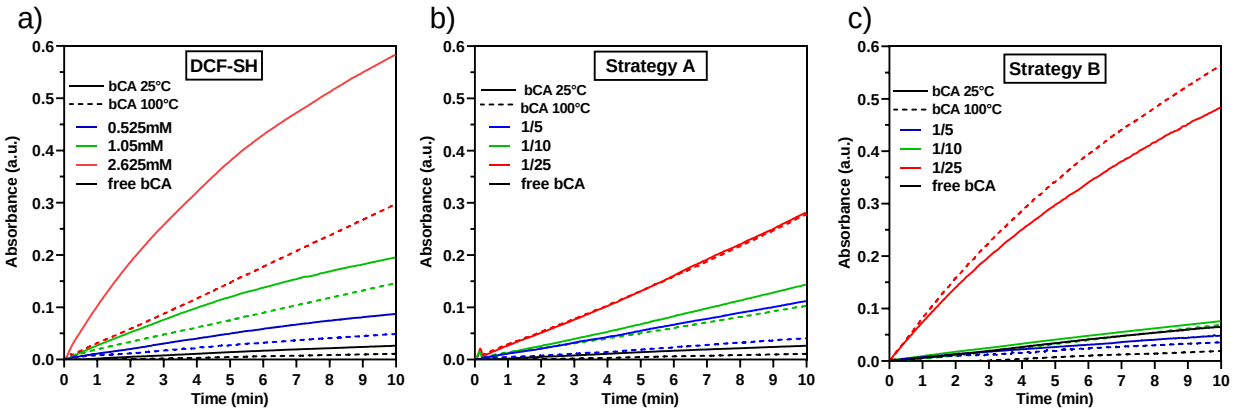

Figure 5. Kinetic hydrolysis experiments at 25°C (line) after incubation for 5h at 100°C(dot line) at different concentrations of a) DCF-SH-bCA and AuNps-DCFs-bCA assembled *via* Strategies b) A and c) B.

Table 1. Kinetic parameters of bCA, K_m and V_{max} determined from Michaelis-Menten model for DCF-PEG and DCF-SH.

DCF-PEG (mM)	K_m (mM)	V_{max} (mM/min)	DCF-SH (mM)	K_m (mM)	V_{max} (mM/min)
0.84	17.0	0.49	**0.84**	12.8	0.55
1.05	14.5	0.55	**1.05**	7.5	0.63
AuNps/DCFs molar ratio	**Strategy A**		**Strategy B**		
	K_m (mM)	V_{max} (mM/min)	K_m (mM)		V_{max} (mM/min)

1/18	14.33	0.84	6.8	1.08

In both cases the growth numbers significantly increase and are proportional to the concentration of DCF-PEG on AuNps surface **(Figure 4h, S16)**, when comparing to DCF-PEG (**Figure 4e**) and NH_2-PEG_{2000}-SHAuNps DCF-PEG (**Figure 4f**). The formation of larger low density aggregates of NH_2-PEG_{2000}-SHAuNps-DCFs as observed by DLS (**Figure 2e**) and the most probable location of the bCA in a DCFs environment avoid direct contacts with AuNps as obtained following the strategy C ensures a more important activation with higher growth numbers than in the AuNps-DCF-SH-bCA systems (Strategies A,B) (**Figure 4i**). In addition, this combination significantly ameliorated bCA activation. The major activity with a growth factor of ~30 is obtained with strategy C2 For the immobilization of bCA at the interface with NH_2-PEG_{2000}-SHAuNps and DCF-PEG constituting the best environment for the activation including high density of DCFs and optimal interactions within the space between particles.

The activation behavior was then quantitatively monitored by determining the K_m equal to the substrate concentration at half of the maximum rate V_{max}, which were both determined by fitting the data with the Michaelis-Menten model (**Figures S17-S19**). As shown in Table 1, the addition of increasing amounts of DCF-PEG or DCF SH decrease the K_m = 23.2 mM of free bCA. The observed decrease is higher for DCF-SH (K_m = 7.5 mM) as compared with DCF-PEG (K_m = 14.5 mM) for a similar V_{max} ~ 0.5 $mM.min^{-1}$ for both DCFs immobilizing bCA. Previous studies indicate that lower K_m and unchanged V_{max} reveal a stronger affinity with the bCA under DCF-confinement [42,43]. It indicates that enzyme activation meaning increased intrinsic catalytic efficiency (isochorismate enzyme) is provided by a macromolecular crowding effect within DCFs matrices *via* particularly imine or disulfide connection reversible bonds interconnected with flexible PEG chains non-covalently interacting with the enzyme surface. This is lowering its dynamics under confined conditions to fit the best in presence of substrate, while maintaining its conformation as described previously in fluorescence studies. DCFs made of polyethylenimine (PEI) exhibited a comparable reduction in K_m, approximately 2-fold, with a value of 2.08 mM, compared to 3.13 mM for free bCA [44]. We know that activator molecule participates to the rate-determining step of the CA catalytic cycle, i.e., proton shuttling between the Zn^{2+}-H_2O and the exterior, leading to Zn^{2+}-OH^- species in the enzyme pocket [21,25]. The present dynamers decorated with imines/amines are able to participate in proton shuttling which facilitate the formation of the nucleophilic species of the enzyme, explaining thus their highly efficient activating properties. We have previously shown [25] that the PEG backbones were responsible only for general encapsulation in a whole leading to the change of enzyme secondary structure, supported by CD spectra[25], while the functional amine groups on dynamers were the main reason for H^+ shuttling activation.

The K_m value of AuNps-DCFs-bCA bioconjugates assembled *via* strategies A and B were two and three times respectively, lower than free bCA less indicating stronger affinity with the enzyme under confinement **(Table 1)**. The V_{max} increased significantly to 0.84 mM/min (A) and 1.08 mM/min (B) respectively, meaning that more active enzymes are implicated. An efficient activator of CA, timolol, showed a two times increase in V_{max}, which accelerates the catalytic activity [45].

Temperature is an important parameter that can change the conformation of proteins, especially when the active enzymes as bCA are used under harsh conditions like flue gas CO_2 capture. We determined the thermal stability of free bCA and encapsulated AuNps-DCFs-bCA at 25 ºC and 100 ºC. At high concentrations, the activity of DCF-SH-bCA is diminished by 50%, while for AuNps-DCFs-bCA bioconjugates the activity is 100% maintained at 100 ºC, when compared to 25 ºC **(Figure 5)**. Importantly, AuNps play an important role in protecting bCA from denaturation within the conjugates providing an important increasing interest to use these systems under harsh condition required by industrial CO_2 capture processes operated at high temperatures.

CONCLUSIONS

In conclusion, we have discovered that multivalent DCFs AuNps conjugates are interesting host matrixes to enhance the bCA enzyme catalytic activity by changing the enzyme microenvironment. The two approaches adapted succeeded to form cross-linked bioconjugates at the nanoscale. First, the "grafting to" approach yielded to the interconnection of citrate-stabilized AuNps of 22 nm into denser low dimensional aggregates of 80 - 160 nm diameter in presence of DCF-SH, whereas the second, the "grafting from" approach, induced the formation of bigger assemblies of 200 nm between NH_2-PEG_{2000}-SHAuNps and DCF-PEG. The results obtained in this work showed that multivalent presentation of AuNps-DCFs-bCA components within nanoscaled platforms present outstanding and optimal binding behaviors triggering structural changes within bCA, which results in an impressive improved catalytic activity under confined conditions, more than 30 times higher than bCA alone. The AuNps-DCFs-bCA nanohybrid biocatalysts were notably robust and able to provide catalytic activation effects after being exposed to relatively harsh temperature of 100°C making them useful for their feasible deployment in real systems for CO_2 capture requesting materials to maintain high performance at such temperatures.

ASSOCIATED CONTENT

Supporting Information

General information on Au NPs and DCF Au NPS synthesis. Characterization of DCFs: DLS,, FTIR, Catalytic activity determination This material is available free of charge via the Internet at http://pubs.acs.org.

AUTHOR INFORMATION

Corresponding Author

* Mihail Barboiu - Institut Européen des Membranes, Adaptive Supramolecular, Nanosystems Group, University of Montpellier, ENSCM, CNRS, Place Eugène Bataillon, CC 047, F-34095, Montpellier, France and Babes-Bolyai University, Supramolecular Organic and Organometallic Chemistry Center (SOOMCC), Cluj-Napoca, 11 Arany Janos str., 400028, Cluj-Napoca, Romania. E-mail: mihail-dumitru.barboiu@umontpellier.fr

Authors

Sanaa Daakour - Institut Européen des Membranes, Adaptive Supramolecular, Nanosystems Group, University of Montpellier, ENSCM, CNRS, Place Eugène Bataillon, CC 047, F-34095, Montpellier, France; Bioactive Molecules Research Laboratory, Department of Chemistry and Biochemistry, Faculty of Sciences, Section II, Lebanese University, Jdaidet el-Metn, B.P. 90656, Lebanon.

Gihane Nasr - Bioactive Molecules Research Laboratory, Department of Chemistry and Biochemistry, Faculty of Sciences, Section II, Lebanese University, Jdaidet el-Metn, B.P. 90656, Lebanon.

Author Contributions

The manuscript was written through contributions of all authors. / All authors have given approval to the final version of the manuscript.

ACKNOWLEDGMENT

This work was supported by M-ERA NET 2019 SMARTMATTER grant via Agence Nationale de la Recherche ANR-20-MERA-0001-01 and the project "Evolution" funded by European Union – NextgenerationEU and Romanian Government, under National Recovery and Resilience Plan for Romania, contract no.760033/23.05.2023/23.05.2023, cod PNRR-C9-I8-CF16, through the Romanian Ministry of Research, Innovation and Digitalization, within Component 9, Investment I8".

REFERENCES

(1) Barboiu, M. *Constitutional Dynamic Chemistry*; Springer Science & Business Media, 2012.

(2) Zhang, Y.; Qi, Y.; Ulrich, S.; Barboiu, M.; Ramström, O. Dynamic Covalent Polymers for Biomedical Applications. *Mat. Chem. Front.* **2020**, *4* (2), 489–506.

(3) Fialkowski, M.; Bishop, K. J. M.; Klajn, R.; Smoukov, S. K.; Campbell, C. J.; Grzybowski, B. A. Principles and Implementations of Dissipative (Dynamic) Self-Assembly. *J. Phys. Chem. B* **2006**, *110* (6), 2482–2496.

(4) Bishop, K. J. M.; Wilmer, C. E.; Soh, S.; Grzybowski, B. A. Nanoscale Forces and Their Uses in Self-Assembly. *Small* **2009**, *5* (14), 1600–1630.

(5) Han, Y.; Nowak, P.; Colomb-Delsuc, M.; Leal, M. P.; Otto, S. Instructable Nanoparticles Using Dynamic Combinatorial Chemistry. *Langmuir* **2015**, *31* (46), 12658–12663.

(6) Zhang, Y.; Barboiu, M. Constitutional Dynamic Materials—Toward Natural Selection of Function. *Chem. Rev.* **2016**, *116* (3), 809–834.

(7) Lehn, J.-M. From Supramolecular Chemistry towards Constitutional Dynamic Chemistry and Adaptive Chemistry. *Chem. Soc. Rev.* **2007**, *36* (2), 151–160.

(8) Catana, R.; Barboiu, M.; Moleavin, I.; Clima, L.; Rotaru, A.; Ursu, E.-L.; Pinteala, M. Dynamic Constitutional Frameworks for DNA Biomimetic Recognition. *Chem. Comm.* **2015**, *51* (11), 2021–2024.

(9) Olson, E.; Liu, F.; Blisko, J.; Li, Y.; Tsyrenova, A.; Mort, R.; Vorst, K.; Curtzwiler, G.; Yong, X.; Jiang, S. Self-Assembly in Biobased Nanocomposites for Multifunctionality and Improved Performance. *Nano. Adv.* **2021**, *3* (15), 4321–4348.

(10) Eustis, S.; A. El-Sayed, M. Why Gold Nanoparticles Are More Precious than Pretty Gold: Noble Metal Surface Plasmon Resonance and Its Enhancement of the Radiative and Nonradiative Properties of Nanocrystals of Different Shapes. *Chem. Soc. Rev.* **2006**, *35* (3), 209–217.

(11) Li, D.; He, Q.; Li, J. Smart Core/Shell Nanocomposites: Intelligent Polymers Modified Gold Nanoparticles. *Adv. Coll. Interf. Sci.* **2009**, *149* (1), 28–38.

(12) Boal, A. K.; Ilhan, F.; DeRouchey, J. E.; Thurn-Albrecht, T.; Russell, T. P.; Rotello, V. M. Self-Assembly of Nanoparticles into Structured Spherical and Network Aggregates. *Nature* **2000**, *404* (6779), 746–748.

(13) Frankamp, B. L.; Boal, A. K.; Rotello, V. M. Controlled Interparticle Spacing through Self-Assembly of Au Nanoparticles and Poly (Amidoamine) Dendrimers. *J. Am. Chem. Soc.* **2002**, *124* (51), 15146–15147.

(14) Nowak, P.; Saggiomo, V.; Salehian, F.; Colomb-Delsuc, M.; Han, Y.; Otto, S. Localized Template-Driven Functionalization of Nanoparticles by Dynamic Combinatorial Chemistry. *Angew. Chem. Int. Ed.* **2015**, *54* (14), 4192–4197.

(15) della Sala, F.; Kay, E. R. Reversible Control of Nanoparticle Functionalization and Physicochemical Properties by Dynamic Covalent Exchange. *Angew. Chem. Int. Ed.* **2015**, *54* (14), 4187–4191.

(16) Tao, Y.; Ju, E.; Ren, J.; Qu, X. Polypyrrole Nanoparticles as Promising Enzyme Mimics for Sensitive Hydrogen Peroxide Detection. *Chem. Comm.* **2014**, *50* (23), 3030–3032.

(17) Garcia-Galan, C.; Berenguer-Murcia, Á.; Fernandez-Lafuente, R.; Rodrigues, R. C. Potential of Different Enzyme Immobilization Strategies to Improve Enzyme Performance. *Adv. Synth. Catal.* **2011**, *353* (16), 2885–2904.

(18) You, Y.; Deng, Q.; Wang, Y.; Sang, Y.; Li, G.; Pu, F.; Ren, J.S.; Qu, X. DNA-Based Platform for Efficient and Precisely Targeted Bioorthogonal Catalysis in Living Systems. *Nat Commun* **2022**, *13* (1), 1459.

(19) San, B. H.; Kim, S.; Moh, S. H.; Lee, H.; Jung, D.-Y.; Kim, K. K. Platinum Nanoparticles Encapsulated by Aminopeptidase: A Multifunctional Bioinorganic Nanohybrid Catalyst. *Ang. Chem.* **2011**, *50*, 11924–11929.

(20) Liu, X.; Zhang, Z.; Zhang, Y.; Guan, Y.; Liu, Z.; Ren, J.; Qu, X. Artificial Metalloenzyme-Based Enzyme Replacement Therapy for the Treatment of Hyperuricemia. *Adv. Funct. Mat.* **2016**, *26* (43), 7921–7928.

(21) Supuran, C. T. Carbonic Anhydrases: From Biomedical Applications of the Inhibitors and Activators to Biotechnological Use for CO2 Capture. *J. Enz. Inhib. Med. Chem.* **2013**, *28* (2), 229–230.

(22) Ren, S.; Jiang, S.; Yan, X.; Chen, R.; Cui, H. Challenges and Opportunities: Porous Supports in Carbonic Anhydrase Immobilization. *J. CO2 Utiliz* **2020**, *42*, 101305.

(23) Crumbliss, A. L.; Perine, S. C.; Stonehuerner, J.; Tubergen, K. R.; Zhao, J.; Henkens, R. W.; O'Daly, J. P. Colloidal Gold as a Biocompatible Immobilization Matrix Suitable for the Fabrication of Enzyme Electrodes by Electrodeposition. *Biotech. Bioeng.* **1992**, *40* (4), 483–490.

(24) Vinoba, M.; Lim, K. S.; Lee, S. H.; Jeong, S. K.; Alagar, M. Immobilization of Human Carbonic Anhydrase on Gold Nanoparticles Assembled onto Amine/Thiol-Functionalized Mesoporous SBA-15 for Biomimetic Sequestration of CO2. *Langmuir* **2011**, *27* (10), 6227–6234.
(25) Zhang, Y.; Legrand, Y.-M.; Petit, E.; Supuran, C. T.; Barboiu, M. Dynamic Encapsulation and Activation of Carbonic Anhydrase in Multivalent Dynameric Host Matrices. *Chem. Comm.* **2016**, *52* (21), 4053–4055.
(26) Turkevich, J.; Stevenson, P. C.; Hillier, J. A Study of the Nucleation and Growth Processes in the Synthesis of Colloidal Gold. *Discuss. Farad. Soc.* **1951**, *11*, 55–75.
(27) Cleland, J. L.; Hedgepeth, C.; Wang, D. I. Polyethylene Glycol Enhanced Refolding of Bovine Carbonic Anhydrase B. Reaction Stoichiometry and Refolding Model. *J. Bio. Chem.* **1992**, *267* (19), 13327–13334.
(28) Xia, X.; Yang, M.; Wang, Y.; Zheng, Y.; Li, Q.; Chen, J.; Xia, Y. Quantifying the Coverage Density of Poly (Ethylene Glycol) Chains on the Surface of Gold Nanostructures. *ACS nano* **2012**, *6* (1), 512–522.
(29) Latham, A. H.; Williams, M. E. Versatile Routes toward Functional, Water-Soluble Nanoparticles via Trifluoroethylester–PEG–Thiol Ligands. *Langmuir* **2006**, *22* (9), 4319–4326.
(30) Blakey, I.; Merican, Z.; Thurecht, K. J. A Method for Controlling the Aggregation of Gold Nanoparticles: Tuning of Optical and Spectroscopic Properties. *Langmuir* **2013**, *29* (26), 8266–8274.
(31) Li, D.; He, Q.; Cui, Y.; Duan, L.; Li, J. Immobilization of Glucose Oxidase onto Gold Nanoparticles with Enhanced Thermostability. *Biochem. biophys. res. comm.* **2007**, *355* (2), 488–493.
(32) Dong, J.; Carpinone, P. L.; Pyrgiotakis, G.; Demokritou, P.; Moudgil, B. M. Synthesis of Precision Gold Nanoparticles Using Turkevich Method. *KONA Pow. Part. J.* **2020**, *37*, 224–232.
(33) Lee, P. C.; Meisel, D. Surface-Enhanced Raman Scattering of Colloid-Stabilizer Systems. *Chem. Phy. Lett.* **1983**, *99* (3), 262–265.
(34) Wang, W.; Wei, Q.-Q.; Wang, J.; Wang, B.-C.; Zhang, S.; Yuan, Z. Role of Thiol-Containing Polyethylene Glycol (Thiol-PEG) in the Modification Process of Gold Nanoparticles (AuNPs): Stabilizer or Coagulant? *J. coll. inter. sci.* **2013**, *404*, 223–229.
(35) Abdelhalim, M. A. K.; M. Mady, M. Physical Properties of Different Gold Nanoparticles: Ultraviolet-Visible and Fluorescence Measurements. *J Nano. Nanotech.* **2012**, *03* (03), 178-194.
(36) Corbierre, M. K.; Cameron, N. S.; Sutton, M.; Mochrie, S. G. J.; Lurio, L. B.; Rühm, A.; Lennox, R. B. Polymer-Stabilized Gold Nanoparticles and Their Incorporation into Polymer Matrices. *J. Am. Chem. Soc.* **2001**, *123* (42), 10411–10412.
(37) Sułkowska, A. Interaction of Drugs with Bovine and Human Serum Albumin. *J. Mol. Struct.* **2002**, *614* (1), 227–232.
(38) Teale, F. W. J.; Weber, G. Ultraviolet Fluorescence of the Aromatic Amino Acids. *Biochem J* **1957**, *65* (3), 476–482.
(39) Iosin, M.; Toderas, F.; Baldeck, P. L.; Astilean, S. Study of Protein–Gold Nanoparticle Conjugates by Fluorescence and Surface-Enhanced Raman Scattering. *J. Mol. Struct.* **2009**, *924–926*, 196–200.
(40) Lakowicz, J. R. *Principles of Fluorescence Spectroscopy*, 3rd ed.; Springer: New York, 2006.
(41) Zhang, Y.; Barboiu, M.; Ramström, O.; Chen, J. Surface-Directed Selection of Dynamic Constitutional Frameworks as an Optimized Microenvironment for Controlled Enzyme Activation. *ACS Catal.* **2020**, *10* (2), 1423–1427.
(42) Jiang, M.; Guo, Z. Effects of Macromolecular Crowding on the Intrinsic Catalytic Efficiency and Structure of Enterobactin-Specific Isochorismate Synthase. *J. Am. Chem. Soc.* **2007**, *129* (4), 730–731.
(43) Xue, T.; Jiang, S.; Qu, Y.; Su, Q.; Cheng, R.; Dubin, S.; Chiu, C.-Y.; Kaner, R.; Huang, Y.; Duan, X. Graphene-Supported Hemin as a Highly Active Biomimetic Oxidation Catalyst. *Ang. Chem. Int. Ed.* **2012**, *51* (16), 3822–3825.
(44) Su, D.-D.; Aissou, K.; Zhang, Y.; Gervais, V.; Ulrich, S.; Barboiu, M. Squalene–Polyethyleneimine–Dynamic Constitutional Frameworks Enhancing the Enzymatic Activity of Carbonic Anhydrase. *Catal. Sci.Techn.* **2022**, *12* (10), 3094–3101.
(45) Sugimoto, A.; Ikeda, H.; Tsukamoto, H.; Kihira, K.; Ishioka, M.; Hirose, J.; Hata, T.; Fujioka, H.; Ono, Y. Timolol Activates the Enzyme Activities of Human Carbonic Anhydrase I and II. *Bio. Pharm. Bull.* **2010**, *33* (2), 301–306.

SYNOPSIS TOC